

An experimental and numerical investigation of coarse aggregate settlement in fresh concrete under vibration

Cai, Yuxin; Liu, Qing feng; Yu, Linwen; Meng, Zhaozheng ; Hu, Zhe; Yuan, Qiang ; Šavija, Branko

DOI

[10.1016/j.cemconcomp.2021.104153](https://doi.org/10.1016/j.cemconcomp.2021.104153)

Publication date

2021

Document Version

Accepted author manuscript

Published in

Cement and Concrete Composites

Citation (APA)

Cai, Y., Liu, Q. F., Yu, L., Meng, Z., Hu, Z., Yuan, Q., & Šavija, B. (2021). An experimental and numerical investigation of coarse aggregate settlement in fresh concrete under vibration. *Cement and Concrete Composites*, 122, Article 104153. <https://doi.org/10.1016/j.cemconcomp.2021.104153>

Important note

To cite this publication, please use the final published version (if applicable).
Please check the document version above.

Copyright

Other than for strictly personal use, it is not permitted to download, forward or distribute the text or part of it, without the consent of the author(s) and/or copyright holder(s), unless the work is under an open content license such as Creative Commons.

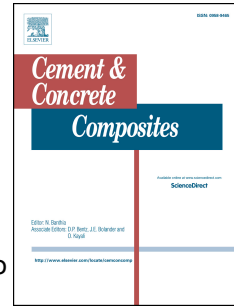
Takedown policy

Please contact us and provide details if you believe this document breaches copyrights.
We will remove access to the work immediately and investigate your claim.

Journal Pre-proof

An experimental and numerical investigation of coarse aggregate settlement in fresh concrete under vibration

Yuxin Cai, Qing-feng Liu, Linwen Yu, Zhaozheng Meng, Zhe Hu, Qiang Yuan, Branko Šavija



PII: S0958-9465(21)00221-3

DOI: <https://doi.org/10.1016/j.cemconcomp.2021.104153>

Reference: CECO 104153

To appear in: *Cement and Concrete Composites*

Received Date: 21 April 2021

Revised Date: 10 June 2021

Accepted Date: 21 June 2021

Please cite this article as: Y. Cai, Q.-f. Liu, L. Yu, Z. Meng, Z. Hu, Q. Yuan, B. Šavija, An experimental and numerical investigation of coarse aggregate settlement in fresh concrete under vibration, *Cement and Concrete Composites* (2021), doi: <https://doi.org/10.1016/j.cemconcomp.2021.104153>.

This is a PDF file of an article that has undergone enhancements after acceptance, such as the addition of a cover page and metadata, and formatting for readability, but it is not yet the definitive version of record. This version will undergo additional copyediting, typesetting and review before it is published in its final form, but we are providing this version to give early visibility of the article. Please note that, during the production process, errors may be discovered which could affect the content, and all legal disclaimers that apply to the journal pertain.

© 2021 Published by Elsevier Ltd.

An experimental and numerical investigation of coarse aggregate settlement in fresh concrete under vibration

Yuxin Cai ^{a,b}, Qing-feng Liu ^{a,b,*}, Linwen Yu ^c, Zhaozheng Meng ^{a,b}, Zhe Hu ^{a,b},
Qiang Yuan ^d, Branko Šavija ^e

^a State Key Laboratory of Ocean Engineering, School of Naval Architecture, Ocean and Civil Engineering, Shanghai Jiao Tong University, Shanghai 200240, China

^b Shanghai Key Laboratory for Digital Maintenance of Buildings and Infrastructure, Shanghai 200240, China

^c College of Materials Science and Engineering, Chongqing University, Chongqing 400045, China

^d School of Civil Engineering, Central South University, Changsha 410075, China

^e Microlab, Faculty of Civil Engineering and Geosciences, Delft University of Technology, Delft 2628CN, the Netherlands

* Corresponding author.

E-mail address: liuqf@sjtu.edu.cn (Q.-F. Liu).

Abstract

Fresh concrete needs vibration to compact, fill the mould and reach a dense state. During the compaction process, coarse aggregates (CAs) tend to settle, affecting the homogeneity and eventually the long-term durability of hardened concrete. In this study, a 3-D, multi-phase numerical model for fresh concrete is developed for better understanding the CA settlement under vibration. The settlement rate of the CA in vibrated concrete is considered based on the Stokes law, and the calibrated rheological parameter of mixtures is determined by the segmented sieving method. The model prediction shows that the vibration time has the greatest effect on CA settlement, followed by the particle size of CAs, whereas the density of CAs and the plastic viscosity of mixtures contribute a little compared with the aforementioned factors. Through experimental tests, the validity of prediction results is well verified. The proposed model provides a new method to understand and estimate the settlement behaviour of CAs.

Keywords: CA settlement; Fresh concrete; Vibration; Rheology; Numerical model; Grey relational analysis

1. Introduction

In general, concrete comprises cement as a binder, natural sand and gravel as aggregates, and mixing water together with chemical admixtures. With the hydration reaction of cementitious materials, fresh concrete will gradually develop from a viscoplastic cohesive process to a viscoelastic hardening process [1]. The stability of fresh concrete refers to its ability to maintain the uniform distribution of constituents during transport, casting and compacting [2]. In the process of consolidation, vibration helps to remove entrapped air voids and improve the compactness of concrete, but also causes the relative movement and redistribution of various components of mixtures due to the insufficient cohesion and density difference [3,4]. Notably, high-frequency vibration-induced settlement of coarse aggregates (CAs) greatly increases the heterogeneity of fresh concrete [5–7]. At present, among various types of concretes, only self-compacting concrete with optimum flowability and viscosity does not need to be vibrated during placement [8]. It can be seen that the vibrating process still remains a necessary step in most cases.

The rheological behaviour of vibrated fresh concrete has been reported in some previous studies. Tattersall and Baker [9,10] held the view that fresh concrete no longer behaved as a Bingham model when exposed to vibration, but approximately followed a power-law pseudoplastic model with zero yield value. When the shear rate was rather low, it could be considered as a Newtonian fluid. Hu and de Larrard [11] pointed out that vibration greatly decreased the yield stress, and sometimes even made it practically disappear, which caused the CAs to settle. Nevertheless, the plastic

23 viscosity was reduced a little or seemed unaffected sometimes by external vibration.
24 Esmailkhanian et al. [12] indicated that vibration would decrease the “internal
25 friction” of concrete mixtures, which promoted sinking of CAs under the action of
26 gravity. Pichler et al. [13] highlighted again that the apparent flowing behaviour of
27 fresh cement-based materials under vibration could be described using a power-law
28 model with shear-thinning nature.

29 The settlement of CAs has an adverse impact on the surface appearance, design
30 strength and durability of hardened concrete. This may cause significant problems,
31 such as the decline in mechanical strength, increased shrinkage and cracking, and the
32 reduction of chemical erosion resistance, all of which are detrimental to the
33 performance of reinforced concrete structures [14–21]. However, due to the opacity of
34 concrete, the direct observation of CA settlement with naked eye is impossible.
35 Therefore, some special experimental techniques have been proposed to characterize
36 the settlement phenomenon. Petrou et al. [22] introduced a radioactive element
37 labelling method that utilized nuclear medicine technology to monitor the deposition
38 of CAs in vibrated concrete. Koch et al. [23] and Tian et al. [24] used carbomer gel to
39 prepare a transparent paste, and visually observed the settlement and segregation of
40 fresh concrete. After concrete hardening, Barbosa et al. [25], Navarrete and Lopez
41 [26], and Nili et al. [27] cut the specimen and analysed the CA distribution through
42 image processing. Benaicha et al. [28] proposed a method based on the ultrasonic
43 velocity to estimate the homogeneity and quality of concrete at early age. Through the
44 electrical conductivity method, Khayat et al. [29] inserted the electrode pairs at

45 different heights of concrete specimen to assess the uniformity of CA content.
46 Furthermore, a technique of gamma-ray attenuation was adapted by Vanhove et al. [30]
47 and Gokce et al. [31] to measure the distribution of CAs in concrete.

48 In summary, the instability caused by vibration is a critical issue in fresh concrete,
49 and it is necessary to present a convenient and visual methodology to reveal the
50 problem of CA settlement in vibrated concrete. In recent years, the theoretical models
51 of rheological properties of cement-based materials have been extensively studied
52 [32–37]. However, these developments have not been applied on the evaluation of CA
53 settlement, and most knowledge is still based on experimental observations described
54 above.

55 Therefore, the main objective of this study is to develop a rational and reliable
56 numerical model to investigate the settlement of CAs. Experiments are also designed
57 to verify the validity of the model prediction, based on the segmented sieving method.
58 Parametric studies of influencing factors such as the vibration time, the properties of
59 CAs and the plastic viscosity of mixtures on CA settlement are performed and
60 discussed, and grey relational analysis is put forward to compare the influence level of
61 these factors. The proposed model for CA settlement can not only save time, workload
62 and raw materials, but also provide a potential approach to visualize the CA
63 movement and a complementary tool to adequately understand and estimate the
64 settlement behaviour of CAs in vibrated concrete.

65

66 2. Experimental details

67 2.1. Materials and mixtures

68 P.O 42.5R ordinary Portland cement (OPC) conforming to Chinese standard GB
 69 175-2007 with a density of 3020 kg/m^3 and a Blaine specific surface area of 340
 70 m^2/kg was used to prepare the concrete mixtures. Silica fume (SF), with a density of
 71 2200 kg/m^3 and a Blaine specific surface area of $22205 \text{ m}^2/\text{kg}$, was used to replace a
 72 certain amount of OPC. The chemical compositions of OPC and SF determined by
 73 X-ray fluorescence (XRF) are given in Table 1. River sand was used as the fine
 74 aggregate, with the apparent density of 2690 kg/m^3 , and the fineness modulus of 2.9.
 75 Crushed limestone with a particle size of 5–20 mm was used as the CA, with an
 76 apparent density of 2670 kg/m^3 and approximately regular spherical shape. Particle
 77 size distribution of raw materials is presented in Fig. 1, where OPC and SF were
 78 measured by laser granulometry, and river sand and limestone CA were measured by
 79 sieving method. High-performance polycarboxylate superplasticizer was used in the
 80 mixtures to adjust the workability. Its specific gravity, water reduction rate, solid
 81 content and pH were equal to 1.09, 40%, 42% and 6.7, respectively.

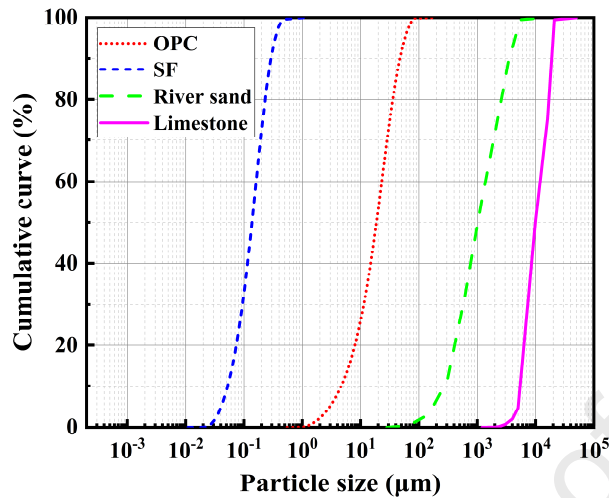
82

83

Table 1 Chemical compositions of OPC and SF (wt%).

Cementitious materials	CaO	SiO ₂	Al ₂ O ₃	Fe ₂ O ₃	MgO	SO ₃	Alkali content	Loss on ignition
	OPC	58.99	22.02	6.19	2.65	2.53	2.67	0.70
SF	0.76	87.42	0.29	1.75	2.49	0.48	–	3.30

84



85

86

Fig. 1. Particle size distribution of raw materials.

87

88

89

90

91

92

93

94

95

96

97

98

99

Prior works [9–11] showed that vibration could change the rheological behaviour of fresh concrete from a thixotropic fluid with yield stress to a non-thixotropic fluid with a very low or even negligible yield stress value. At this time, the CA settlement mainly depended on the plastic viscosity of mixtures and had no relation to the yield stress [8,22,38,39], and a higher viscosity helped decrease the settlement velocity of CAs [40,41]. Hence, three concrete mixtures with different plastic viscosities were designed by adjusting the dosage of SF. The mix proportions of concrete shown in Table 2 were obtained through multiple experiments. Among them, the first was normal concrete (NC), and the second and third added SF to replace 5% and 10% of OPC by mass, respectively, to obtain mixtures with higher plastic viscosities. The water to binder ratio (w/b) was controlled at 0.40, and the dosage of superplasticizer was 0.5% of cementitious materials by mass.

100

101

Table 2 Mix proportions of concrete (kg/m³).

Group	w/b	OPC	SF	River sand	Limestone	Water	Superplasticizer
NC	0.40	400.0	–	736.0	1104.0	160.0	2.0
NC-5%SF	0.40	380.0	20.0	736.0	1104.0	160.0	2.0
NC-10%SF	0.40	360.0	40.0	736.0	1104.0	160.0	2.0

102

103 2.2. Properties of fresh concrete

104

The main properties of these three groups of concrete mixtures are listed in Table

105

3. The apparent density, air content, slump, slump flow and bleeding rate were tested

106

according to the Chinese standard GB/T 50080-2016. The rheological parameters of

107

fresh concrete were measured by the ICAR concrete rheometer produced in Denmark.

108

In the flow curve test, the initial speed is 0.50 rps, the final speed is 0.05 rps, the

109

number of testing points is 7, and the duration of each point is 5 s. The yield stress

110

and plastic viscosity of concrete mixtures were calculated from the flow curve based

111

on the Bingham model, as shown in Eq. (1).

112

$$\tau = \tau_0 + \eta_p \dot{\gamma} \quad (1)$$

113

where τ is the shear stress, τ_0 is the yield stress, η_p is the plastic viscosity, and $\dot{\gamma}$ is

114

the shear rate.

115

116

Table 3 Main properties of fresh concrete.

Group	Apparent density (kg/m ³)	Air content (%)	Slump (mm)	Slump flow (mm)	Bleeding rate (%)	Yield stress (Pa)	Plastic viscosity (Pa·s)
NC	2410	2.5	185	530	5.7	466.2	45.0
NC-5%SF	2400	2.3	175	510	4.9	527.9	48.4
NC-10%SF	2395	2.2	160	490	4.3	560.5	51.3

117

118 2.3. Evaluation of CA settlement

119 A method of segmented sieving was put forward to evaluate the settlement of
 120 CAs in the experiment. The schematic diagram of experimental steps is exhibited in
 121 Fig. 2. Here, a prismatic wooden mould with a cross section of 150 mm × 150 mm
 122 and a height of 500 mm was customized. The wooden boards were fixed by bolts, and
 123 the joints were coated with silicone gel to prevent leakage. A poker vibrator was used
 124 for vibrating and compacting, and its basic parameters are given in Table 4. The
 125 specimens were vibrated for 5 s, 15 s and 25 s, respectively. Note that the effective
 126 working radius of the vibrator used in experiment is 500 mm, which is much larger
 127 than the cross-sectional size of specimen, and the vibrating rod moves across the
 128 entire cross section to work during the vibration. Therefore, it is assumed that the
 129 vibration energy does not attenuate within the range of specimen, that is, the vibration
 130 amplitude and frequency of all particles in fresh concrete are approximately the same.

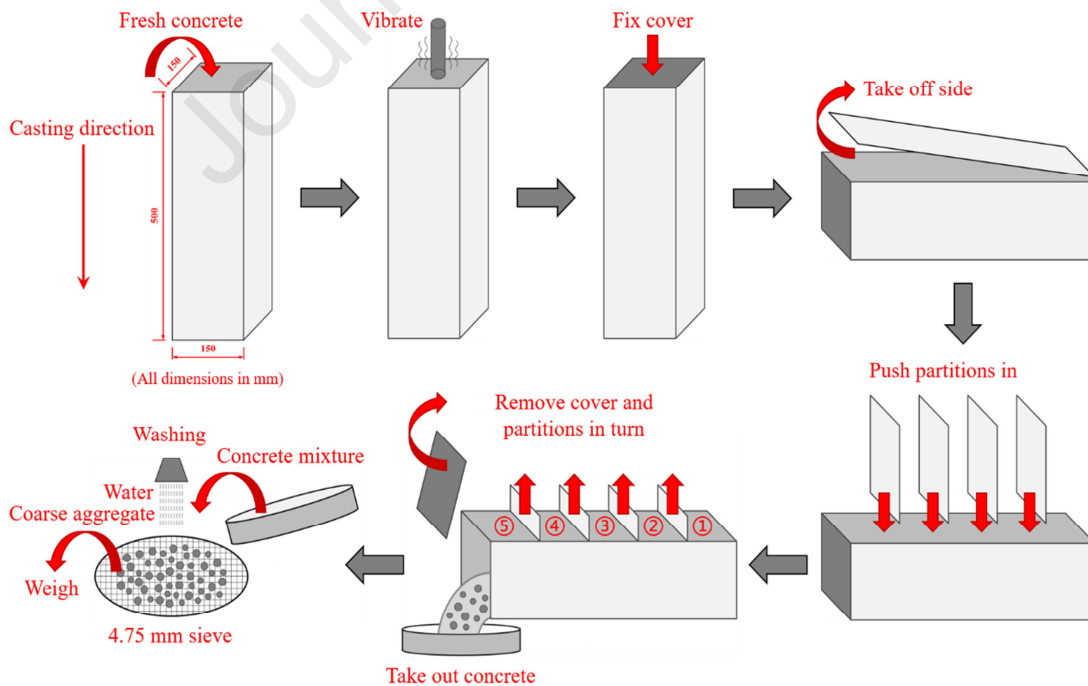
131 In the test, the right amount of fresh concrete was poured into the mould. After

132 the vibration, the top of the mould was covered with a wooden board and fastened
 133 with bolts. Then the mould was slowly rotated by 90° from the original position, and
 134 the side wall was taken off. Next, four pieces of metal slides were inserted vertically
 135 along the designed iron grooves. The concrete mixtures were equally divided in five
 136 layers along the casting direction. Subsequently, the cover and partitions were
 137 removed in proper order. Concrete mixtures of each layer were poured into a 4.75 mm
 138 sieve to rinse to remove mortars. Finally, the residual CAs were dried and weighed to
 139 calculate the CA mass percentage of each layer in the specimen (see Eq. (2)).

$$140 \quad p_i = \frac{m_i}{M} \quad (i = 1, 2, 3, 4, 5) \quad (2)$$

141 where P_i is the mass percentage of CAs in the i -th layer, m_i is the mass of CAs in the
 142 i -th layer, and M is the total mass of all CAs in the specimen.

143



144

145

Fig. 2. Testing procedure of segmented sieving method.

146

147

Table 4 Basic parameters of the poker vibrator.

Type	Rod length (mm)	Rod diameter (mm)	Power (W)	Amplitude (mm)	Frequency (Hz)
YFY-01-35	1000	35	900	0.8	230

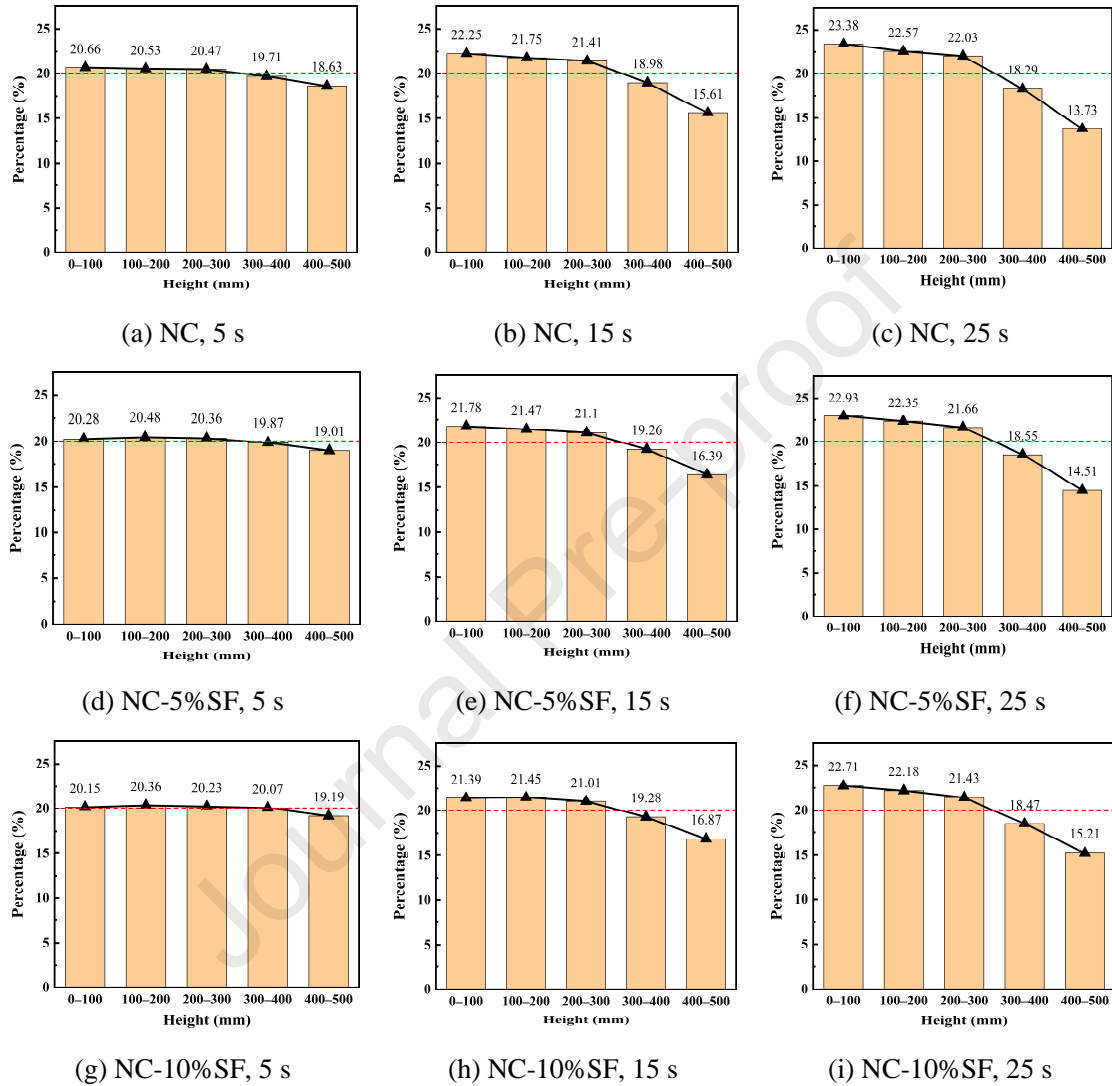
148

149 *2.4. Analysis of experimental results*

150 Fig. 3 illustrates the results of CA distribution along casting direction measured
 151 by the segmented sieving method. In order to eliminate the experimental errors and
 152 ensure the repeatability of this method, each test result was determined by the average
 153 of multiple groups of fresh concrete mixtures. It could be observed that, during the
 154 vibrating procedure, CAs were gradually deposited to the bottom layer of concrete
 155 mixtures under the action of gravity. At the same time, cement pastes and bleeding
 156 water migrated upwards because of the buoyancy. After vibrating, settlement caused a
 157 significant decrease in CA content of the top two layers. For the bottom part of
 158 specimen, the content of CAs increased, but the variation was not as obvious as the
 159 reduction in the top part. It was because a part of CAs gradually formed the close
 160 packing in the bottom area after settling for a certain distance. The subsequent CAs
 161 accumulated in the middle part of specimen, causing the CA mass percentages of the
 162 second and third layers to be close to that of the first layer. The usage of SF could
 163 increase the plastic viscosity of fresh cementitious materials [42–44]. It improved the
 164 stability of fresh concrete and mitigated the settlement of CAs to a certain extent.

165 Besides, the larger dosage of SF had a more significant mitigation effect on
 166 sedimentation phenomenon.

167



168 Fig. 3. Experimental results of CA settlement.

169

170 The degree of CA settlement is defined by the standard deviation of the CA mass
 171 percentage of each layer in the specimen, calculated according to Eq. (3). It can reflect
 172 the overall distribution of CAs, and the higher value indicates that the settlement and
 173 heterogeneous distribution of CAs are more significant.

174

$$S = \sqrt{\frac{\sum_{i=1}^n (P_i - \bar{P})^2}{n}} \times 1000 \quad (3)$$

175

where S is the degree of settlement, P_i is the mass percentage of CAs in the i -th layer,

176

\bar{P} is the average of CA mass percentage of each layer, which is 20%, and n is the

177

number of layers, which is 5.

178

The variation of the settlement degree of CAs with vibration time is displayed in

179

Fig. 4. It could be clearly understood from the figure that once vibration started, CAs

180

appeared unevenly distributed along the casting direction, and the heterogeneity of

181

CA distribution progressively increased. Adding SF into the concrete mixtures could

182

enhance the plastic viscosity, and reduce the settlement degree by 12.67%–45.33%

183

compared with NC. In addition, a part of CAs formed the dense packing and stopped

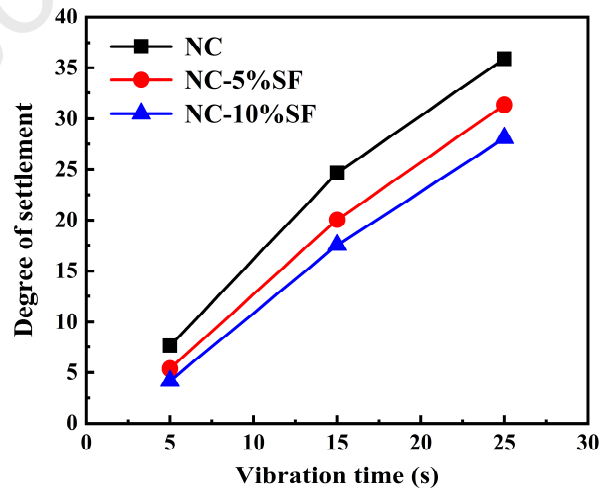
184

moving in the bottom part of specimen after a certain period of vibrating, thereby the

185

increase in the degree of CA settlement gradually weakened with the vibration time.

186



187

188

Fig. 4. Experimental results of the degree of CA settlement.

189

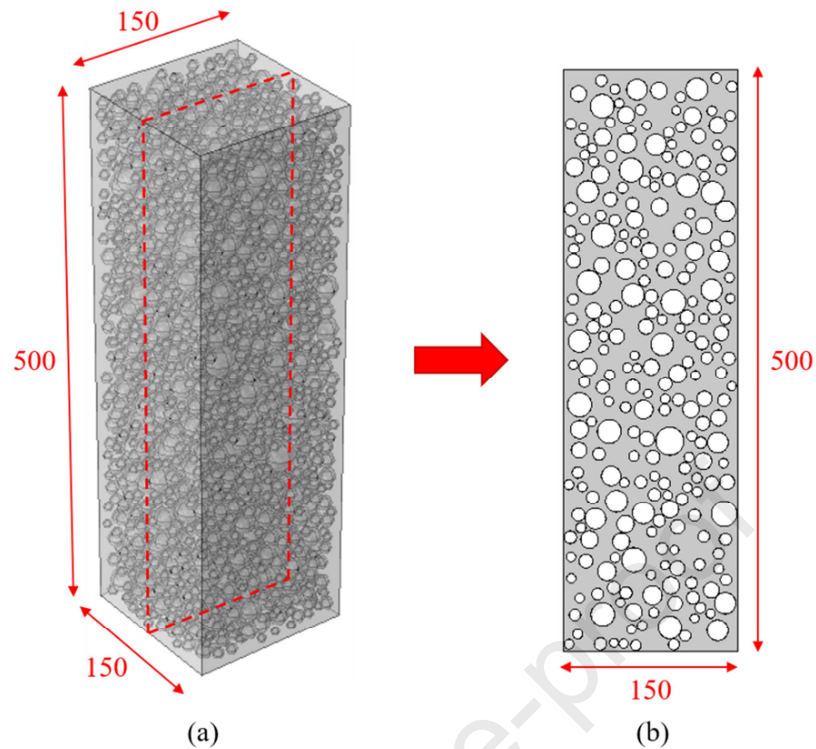
190 **3. Numerical model**

191 *3.1. Modelling approach*

192 Numerical studies can provide accurate models at multiple scales to reflect the
193 material compositions and meso/micro structures of concrete [45–47]. In this study, a
194 3-D fresh concrete model is established at mesoscopic level, as shown in Fig. 5(a).
195 The concrete is considered as a two-phase composite comprising CAs and mortars to
196 facilitate the understanding of the settlement behaviour of CAs. The size of geometric
197 model of the prismatic concrete specimen is 150 mm × 150 mm × 500 mm. The
198 particle size of spherical CAs in the model is 5–20 mm, which is randomly generated
199 according to the Fuller curve, and the volume fraction of CAs is 45%. These
200 parameters are the same as the experiments.

201 Due to the relatively large size of the model, it contains too much CAs, which
202 will block each other in the line of sight. For easier direct observation of the process
203 of CA settlement, we extract some 2-D slices from the 3-D model along the vertical
204 direction and find that the CA settlement in each slice is similar. In consequence, a
205 slice in the middle of 3-D model is extracted vertically for the visual analysis (see Fig.
206 5(b)). Of course, the calculation of CA content distribution is still based on the 3-D
207 model. It can be seen from the figure that after casting and before vibrating, CAs are
208 randomly and uniformly distributed in concrete.

209



210

(a)

(b)

211

Fig. 5. Schematic diagram of geometric model (all dimensions in mm).

212

213

It is generally believed that the yield stress can prevent CAs from settling in an

214

undisturbed mortar matrix [22,39], but the yield stress is known to decrease to a very

215

low value or even disappear at vibrating state and the plastic viscosity plays a decisive

216

role in the settlement of CAs at this time [9–11,48,49]. Assuming that the yield stress

217

is reduced to zero, a single CA particle is mainly subjected to three forces: gravity,

218

buoyancy and viscous resistance in vibrated mortars. The force analysis of the CA is

219

presented in Fig. 6.

220

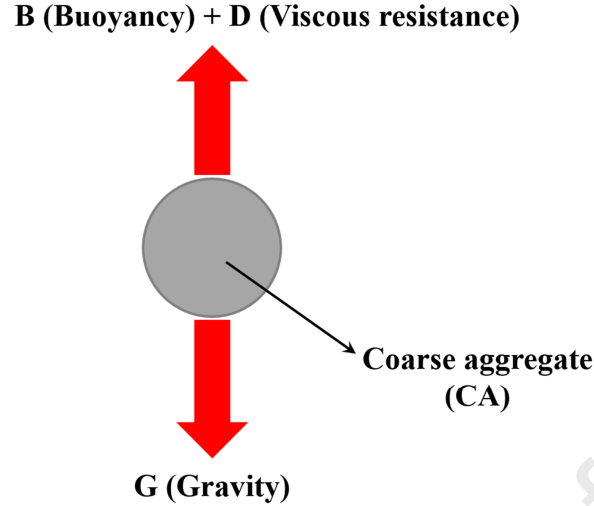


Fig. 6. Force analysis of the CA in vibrated mortars.

Gravity (G) and buoyancy (B) can be expressed as:

$$G = \rho_a V g = \frac{1}{6} \pi \rho_a d^3 g \quad (4)$$

$$B = \rho_m V g = \frac{1}{6} \pi \rho_m d^3 g \quad (5)$$

Here, ρ_a and ρ_m are the apparent densities of CAs and mortars, respectively. In the experiment, ρ_a is 2670 kg/m³. ρ_m is measured on a mortar sample, which is extracted from fresh concrete using a 4.75 mm sieve immediately after the completion of the mixing procedure. The apparent densities of mortars corresponding to the three groups of concrete mixtures are 2285 kg/m³, 2270 kg/m³ and 2260 kg/m³, respectively. d is the diameter of CA particle in the range of 5–20 mm. And g is the acceleration due to gravity, which is 9.8 N/kg.

Stokes law describes the viscous resistance of a spherical object in the viscous fluid. The following assumptions hold: (1) the liquid extends infinitely, that is, the influence of container wall on the fluid movement is not considered; (2) the object is spherical and moves in a straight line with a constant velocity without deformation

238 during the movement; (3) the velocity of liquid on the surface of the sphere relative to
 239 the centre is zero; (4) when the Reynolds number (Re) is small, the inertial effect can
 240 be ignored. Here, Re is a dimensionless parameter that distinguishes the flow type of
 241 fluid and it can be calculated as:

$$242 \quad \text{Re} = \frac{\rho_l v d}{\eta} \quad (6)$$

243 where ρ_l is the fluid density, v is the sphere velocity, d is the sphere diameter, and η is
 244 the fluid viscosity.

245 When Re is less than 1, the flow is considered to be streamlined; when Re is
 246 greater than 10^3 , the flow is turbulent; when Re is between the two, the flow is
 247 transitional. In concrete mixtures, the movement velocity of CA particles is extremely
 248 slow, and Re is much lower than 1. So the flow around the CA particles is streamlined,
 249 and the expression of the viscous resistance (D) is:

$$250 \quad D = 3\pi\eta v d \quad (7)$$

251 From the above analysis, it can be seen that when the density of the CA is greater
 252 than that of the mortars, the CA will move downwards with acceleration, and the
 253 viscous resistance also increases because of the increased CA velocity. When the
 254 resultant force of viscous resistance, gravity and buoyancy reaches an equilibrium, the
 255 CA will settle at a constant velocity. The final velocity can be demonstrated as:

$$256 \quad v_s = \frac{d^2 g (\rho_a - \rho_m)}{18\eta_{pl}} \quad (8)$$

257 where v_s is the final velocity of the CA, and η_{pl} is the plastic viscosity of mortars.

258 The CA in vibrated mortars can be divided into a varying accelerated motion
 259 with a decreasing acceleration and a uniform motion. Through integral calculation, the

260 relationship between the vertical settlement height and vibration time can be derived

261 as:

$$\begin{aligned}
 \Delta h &= \frac{d^2 g (\rho_a - \rho_m)}{18\eta_{pl}} \cdot t - \frac{d^4 g \rho_a (\rho_a - \rho_m)}{324\eta_{pl}^2} \cdot \left[1 - \exp\left(-\frac{18\eta_{pl}}{d^2 \rho_a} \cdot t\right) \right] \\
 &= \frac{d^2 g (\rho_a - \rho_m)}{18\eta_{pl}} \cdot \left\{ t - \frac{d^2 \rho_a}{18\eta_{pl}} \cdot \left[1 - \exp\left(-\frac{18\eta_{pl}}{d^2 \rho_a} \cdot t\right) \right] \right\}
 \end{aligned} \tag{9}$$

263 where Δh is the settlement height of the CA, and t is the vibration time.

264 Since the particle size of CAs in this study is 0.005–0.02 m, the constant and
 265 exponential terms in Eq. (9) are much smaller than the linear term. It can be seen that
 266 the CA will accelerate to the final velocity in a rather short time, which can be ignored.
 267 Moreover, Petrou et al. [39] find that, after the vibration, the yield stress of mortars is
 268 restored immediately, and the dynamic CA will stop moving with a great acceleration
 269 and stabilize in a static state. Hence, the distance of this deceleration motion can also
 270 be ignored. It means that the CA settlement can be approximately regarded as a
 271 uniform motion in the whole process of vibration, and its movement distance is
 272 expressed as:

$$\Delta h = \frac{d^2 g (\rho_a - \rho_m)}{18\eta_{pl}} \cdot t \tag{10}$$

274 Eq. (10) shows the settlement height of a single CA in vibrated mortars. But, in
 275 fact, each CA particle is also subjected to the interaction from other ones. In this case,
 276 the plastic viscosity of mortars can be approximately replaced by that of concrete
 277 mixtures, so as to consider the interaction between the CA particles [50–52].
 278 Furthermore, the plastic viscosity of fresh concrete measured in Section 2.2 needs to
 279 be calibrated, because the Bingham model is no longer completely suitable to

280 characterize the rheology of fresh cement-based materials under the action of
 281 vibration. Consequently, the settlement height of the CA can be revised to:

$$282 \quad \Delta h' = \frac{d^2 g (\rho_a - \rho_m)}{18k\eta_{pl}'} \cdot t \quad (11)$$

283 In Eq. (11), $\Delta h'$ is the actual settlement height of the CA, η_{pl}' is the plastic
 284 viscosity of fresh concrete, and k is the non-dimensional calibration coefficient for η_{pl}' .
 285 The specific value of k will be determined in Section 3.2, which is related to the raw
 286 materials and experimental conditions.

287

288 3.2. Model calibration

289 Theoretically, the final height position of a single CA after settlement can be
 290 expressed by Eq. (12) through the previous calculation and derivation.

$$291 \quad h' = h - \frac{d^2 g (\rho_a - \rho_m)}{18k\eta_{pl}'} \cdot t \quad (12)$$

292 where h is the initial height position of the CA, and h' is the final height position of
 293 the CA after settlement.

294 It should be noted that the CAs with different particle sizes have a different
 295 settlement rate, which will cause some of them to intersect in the model. To this end,
 296 the whole vibration process is divided into many short-time parts, and the vibration
 297 time of each step is set as 0.05 s. The final settlement model is generated by
 298 superposition of each part step by step, until the expected vibration time is reached. At
 299 the end of each part, if the CAs intersect, the involved ones are randomly bounced to
 300 the nearby empty space and ensure that they will not intersect with other CAs again.

301 Considering that the CAs will be wrapped with a layer of pastes (interfacial transition
 302 zone) with a thickness of 20–50 μm [53–55], the minimum distance between the CA
 303 surfaces is set as 100 μm in this study.

304 In the model, the parameter information of every CA particle can be easily
 305 determined at any time and any position. The 3-D model is equally divided into five
 306 layers along the height direction, and all CAs are distributed in each layer based on
 307 the final position of the centre height of them. According to Eq. (13), the CA volume
 308 percentage of each layer in the model can be calculated.

$$309 \quad P_i' = \frac{V_i}{V} (i=1,2,3,4,5) \quad (13)$$

310 where P_i' is the volume percentage of CAs in the i -th layer, V_i is the volume of CAs in
 311 the i -th layer, and V is the total volume of all CAs in the model.

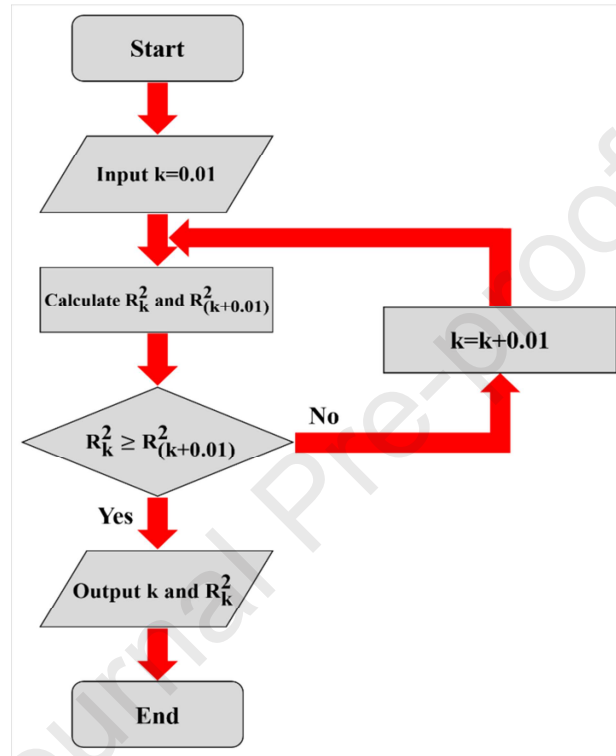
312 Since the density of all CAs is the same, the volume percentage of CAs in each
 313 layer (P_i') can be fitted with the mass percentage (P_i) according to the experimental
 314 results of Fig. 3 to calculate the calibration coefficient (k) used in Eq. (11). The
 315 algorithm flow chart of k and correlation coefficient (R^2) is presented in Fig. 7. R^2 is
 316 calculated by the linear fitting function of software. It can be predicted that the value
 317 of R^2 will increase firstly and then decrease with the increase of k , that is, there is a
 318 peak value of R^2 . When R^2 reaches its maximum value, the algorithm ends. It is found
 319 that when k is 0.62, the results of numerical model and experiment are in the best
 320 agreement. In that case, R^2 is 0.9865. The original data comparison between the
 321 model and experimental results is shown in Table 5, and the fitting result is shown in
 322 Fig. 8. The fitting function is self-set as $y=x$, and the abscissa and ordinate represent

323 the results of experiment and numerical model, respectively. Note that k is less than 1.

324 It means that vibration reduces the plastic viscosity of fresh concrete compared to that

325 in the stable state.

326



327

328

Fig. 7. Algorithm flow chart.

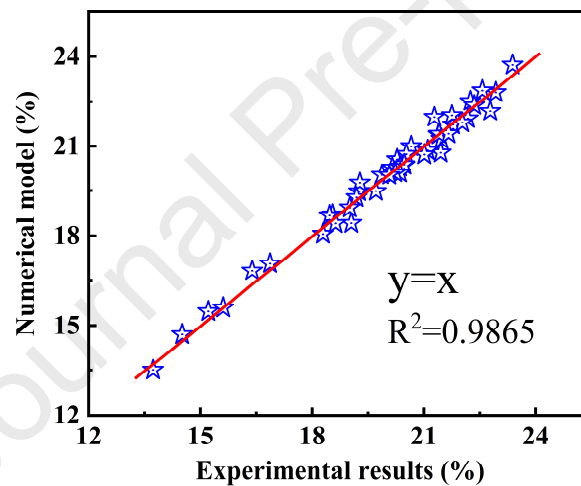
329

330 Table 5 Comparison of the percentage of CA distribution between the model and experiment.

Vibration time	Layer	NC		NC-5%SF		NC-10%SF	
		Model	Experiment	Model	Experiment	Model	Experiment
5 s	1	20.99%	20.66%	20.56%	20.28%	20.28%	20.15%
	2	20.73%	20.53%	20.37%	20.48%	20.31%	20.36%
	3	20.39%	20.47%	20.10%	20.36%	20.11%	20.23%
	4	19.48%	19.71%	20.04%	19.87%	20.03%	20.07%
	5	18.41%	18.63%	18.93%	19.01%	19.27%	19.19%

	1	22.51%	22.25%	21.71%	21.78%	21.38%	21.39%
	2	22.03%	21.75%	21.23%	21.47%	21.05%	21.45%
15 s	3	21.40%	21.41%	20.86%	21.10%	20.72%	21.01%
	4	18.47%	18.98%	19.47%	19.26%	19.77%	19.28%
	5	15.59%	15.61%	16.73%	16.39%	17.08%	16.87%
	1	23.72%	23.38%	22.81%	22.93%	22.27%	22.71%
	2	22.87%	22.57%	22.37%	22.35%	21.92%	22.18%
25 s	3	21.78%	22.03%	21.41%	21.66%	21.67%	21.43%
	4	18.06%	18.29%	18.70%	18.55%	18.67%	18.47%
	5	13.57%	13.73%	14.71%	14.51%	15.47%	15.21%

331



332

333

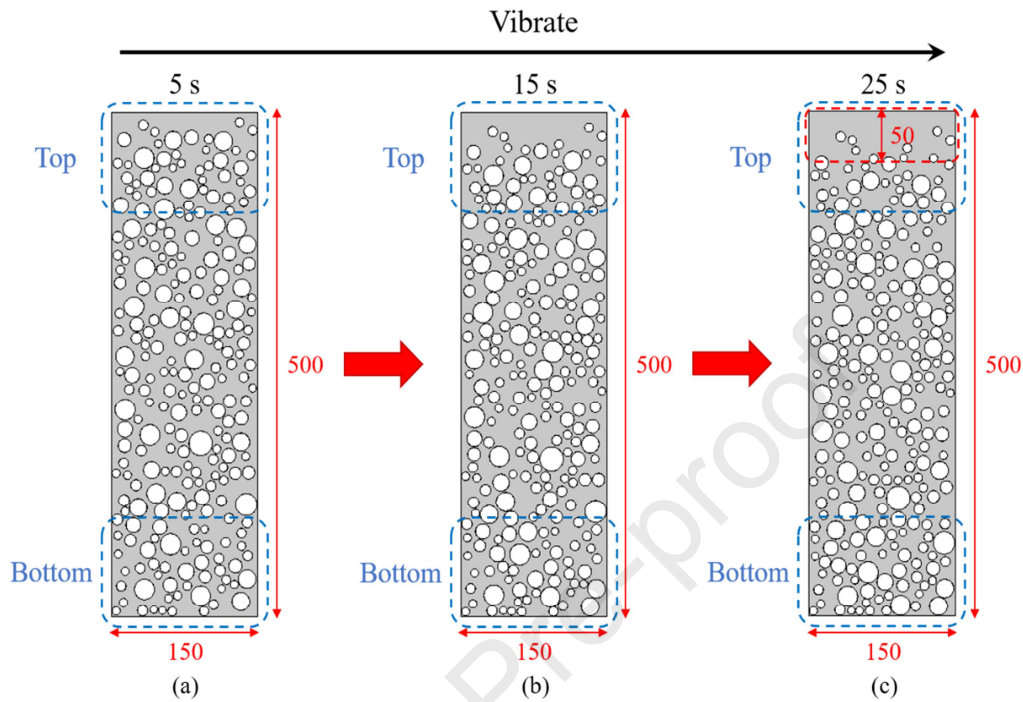
Fig. 8. Fitting between numerical model and experimental results.

334

335 Taking the group of NC as an example, firstly, a 3-D geometric model was
 336 generated, and then a 2-D slice was extracted to facilitate the visual observation of CA
 337 settlement, as depicted in Fig. 9. As the vibration progressed, CAs gradually deposited
 338 to the bottom part of specimen, and the distribution profiles presented an increased
 339 content of CAs towards the bottom layer. For a single CA, the CA with a larger

340 particle size showed a more notable settlement distance.

341



342

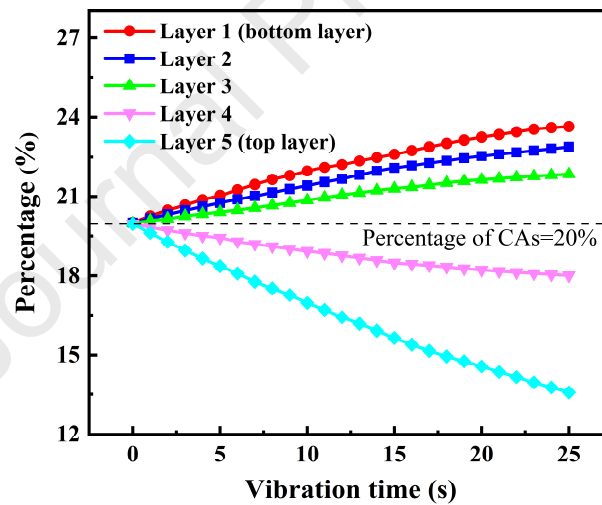
343 Fig. 9. Visual analysis of CA settlement under vibration (all dimensions in mm).

344

345 It was noteworthy that the CA content in the top part of specimen was
 346 significantly decreased, especially when the vibration time reached 25 s, there were
 347 most of mortars and only few of small-sized CAs in the top 50 mm-height area (see
 348 Fig. 9(c)). Megid and Khayat [56] observed similar phenomena in their experiment.
 349 The settlement of CAs led to the formation of a porous surface layer enriched in
 350 cement pastes in the top part of concrete specimen, where might be prone to
 351 experience shrinkage and cracking [57,58]. In addition, it could be clearly seen from
 352 the figure that CAs in the bottom part indeed formed a close packing in the local
 353 space, which confirmed the previous interpretation of the experimental results.

354 On the basis of the 3-D model, the volume percentages of CAs in the five layers

355 were calculated, as illustrated in Fig. 10. Evidently, as the vibration time increased,
 356 the heterogeneity of CA distribution along casting direction was gradually
 357 strengthened, which was reflected in the obvious decrease of CA content in the top
 358 part and the increase of that in the bottom part. This was consistent with the direct
 359 observation shown in Fig. 9. Besides, for concrete mixtures having different w/b or
 360 mix proportions, as long as the relevant rheological parameter of mixtures and raw
 361 material information were input into the model, the CA settlement behaviour could
 362 also be easily displayed. The proposed methodology had potential application
 363 prospects in large-scale structural concrete cast in practice and 3-D printed concrete.
 364



365
 366 Fig. 10. The CA volume percentages of these five layers in NC.

367

368 4. Prediction and discussion

369 The settlement of CAs is a common phenomenon in fresh concrete due to
 370 vibration, and the visually method can provide an important and effective way to
 371 reveal the settlement behaviour of CAs. Based on the numerical approach proposed in

372 this study, a corresponding 3-D model can be established to predict the degree of CA
373 settlement under different influencing factors, for example, the vibration time, the
374 apparent density and particle size of CAs, and the plastic viscosity of mixtures. It not
375 only has the advantages of convenience and visualization, but also can further make a
376 theoretical explanation for such a rheological problem in vibrated concrete.

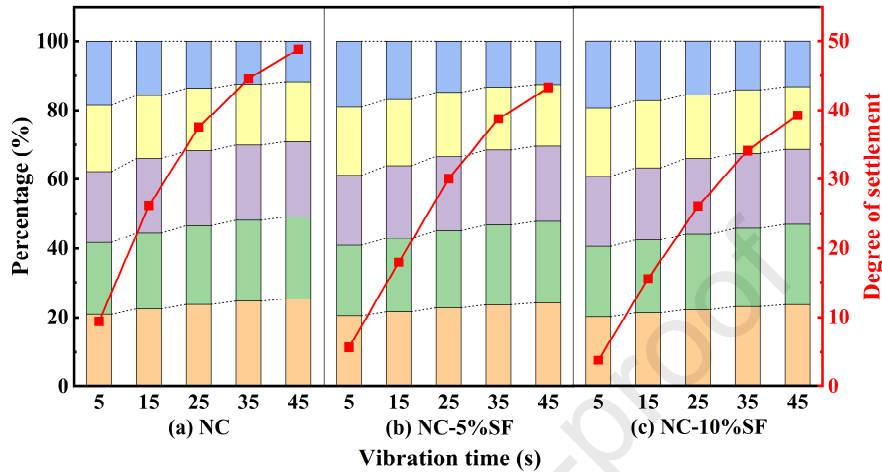
377 *4.1. Influence of vibration time*

378 The distribution of CAs along casting direction under different vibration time is
379 shown in Fig. 11. The orange, green, purple, yellow and blue histograms in the figure
380 represent the volume percentages of CA content from the first layer to the fifth layer
381 of the total, respectively. And the line chart shows the standard deviation of the CA
382 volume percentages of these five layers to characterize the degree of CA settlement
383 (like Eq. (3)). An obvious impact of vibration time on CA settlement could be
384 observed. As the vibrating duration became longer, the heterogeneity of CA
385 distribution gradually increased. After vibrating for a certain period of time, due to the
386 dense packing of some CAs in the bottom part of specimen, the growing trend of
387 settlement degree became slower. It should be noted that the addition of SF would
388 delay the initial time of that a part of CAs in the bottom area formed a close packing.

389 In engineering practice, long-time vibration should be avoided, because
390 excessive vibration would aggravate the settlement, segregation and bleeding of fresh
391 concrete. On the contrary, too short vibration time might make it difficult for each
392 component in mixtures to combine closely and entrapped air voids could not be
393 completely removed from the surface of specimen, which also might affect the quality

394 of hardened concrete. Therefore, when casting fresh concrete, the vibration time
 395 should be strictly controlled, usually 20–30 s.

396



397

398

Fig. 11. Influence of the vibration time on CA settlement.

399

400 4.2. Influence of CA apparent density

401

402

403

404

405

406

407

408

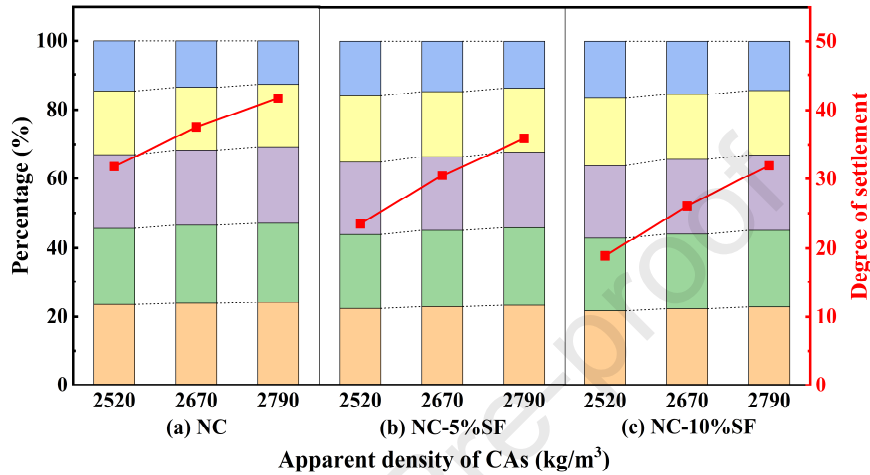
409

410

The properties of CAs, such as apparent density, particle size distribution and appearance shape, may all have a certain influence on the degree of settlement [12,38,59–66]. Considering that the laboratory could offer additional CAs with apparent densities of 2520 kg/m^3 and 2790 kg/m^3 , a numerical model of the influence of apparent density on settlement was carried out, and the vibration time was set as 25 s. From Fig. 12, it showed that the CAs with a larger apparent density presented a higher difference between the densities of the CA and the mortar matrix, resulting in a greater sedimentation tendency. This was in line with the finding of Navarrete and Lopez [59], who believed that the settlement rate had a linear relationship with the density difference between CAs and mortars for a given mixture. Furthermore, Chia et

411 al. [60] and Ke et al. [61] studied the settlement behaviour of lightweight CA concrete
 412 under vibration. They claimed that when the density of CAs was less than that of the
 413 mortars, the CAs would appear to float.

414



415

416

Fig. 12. Influence of the apparent density of CAs on settlement.

417

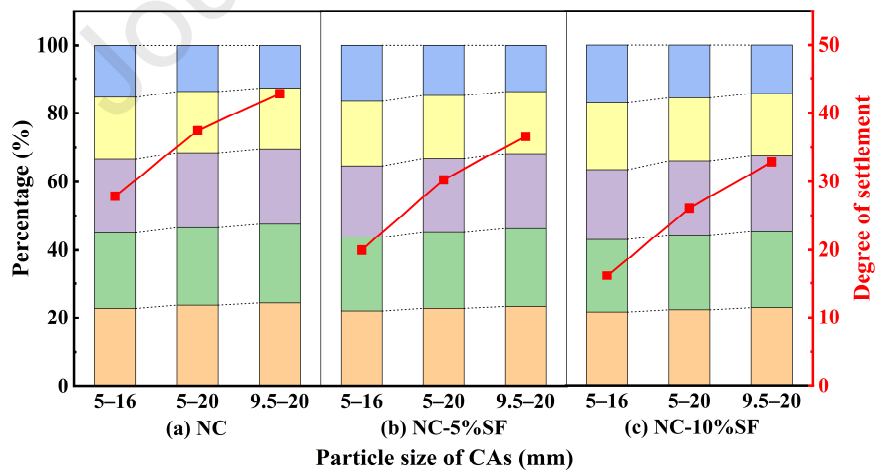
418 4.3. Influence of CA particle size

419 In Fig. 13, three particle size distributions of CAs were designed, namely 5–16
 420 mm, 5–20 mm and 9.5–20 mm, and the vibration time was also 25 s. The reason for
 421 distinguishing the range of particle size in this way was that it could be easily
 422 obtained through the sieves of 9.5 mm and 16 mm sizes in the laboratory, which was
 423 beneficial to the subsequent experimental verification. Under the action of vibration,
 424 the mixtures which contained more large-sized CAs had a greater degree of settlement
 425 for the same CA volume fraction, that was, the distribution of CAs in concrete
 426 presented a more evident non-uniformity. This was consistent with the results of
 427 Safawi et al. [38]. In their experiment, the CAs with particle sizes of 5–13 mm and

428 13–20 mm were used to prepare fresh concrete mixtures, respectively. The results
 429 showed that the large-sized CAs were more affected due to vibration than the
 430 small-sized ones. It meant that the larger-sized CAs were more dominant in
 431 determining the settlement degree compared with smaller ones. Similarly,
 432 Esmailkhanian et al. [12] and Shen et al. [62] also found that concrete mixtures with
 433 lower maximum size CAs tended to settle and segregate less.

434 Moreover, compared with the particle size distribution of CAs which increased
 435 from 5–20 mm to 9.5–20 mm, the increase in the settlement degree of the particle size
 436 from 5–16 mm to 5–20 mm was more obvious. It was because, although the particle
 437 size of CAs increased in both cases, the CAs with a larger particle size were more
 438 likely to form a dense packing when they deposited in the bottom part of specimen,
 439 which could prevent the settlement movement to a certain extent.

440



441

442

Fig. 13. Influence of the particle size of CAs on settlement.

443

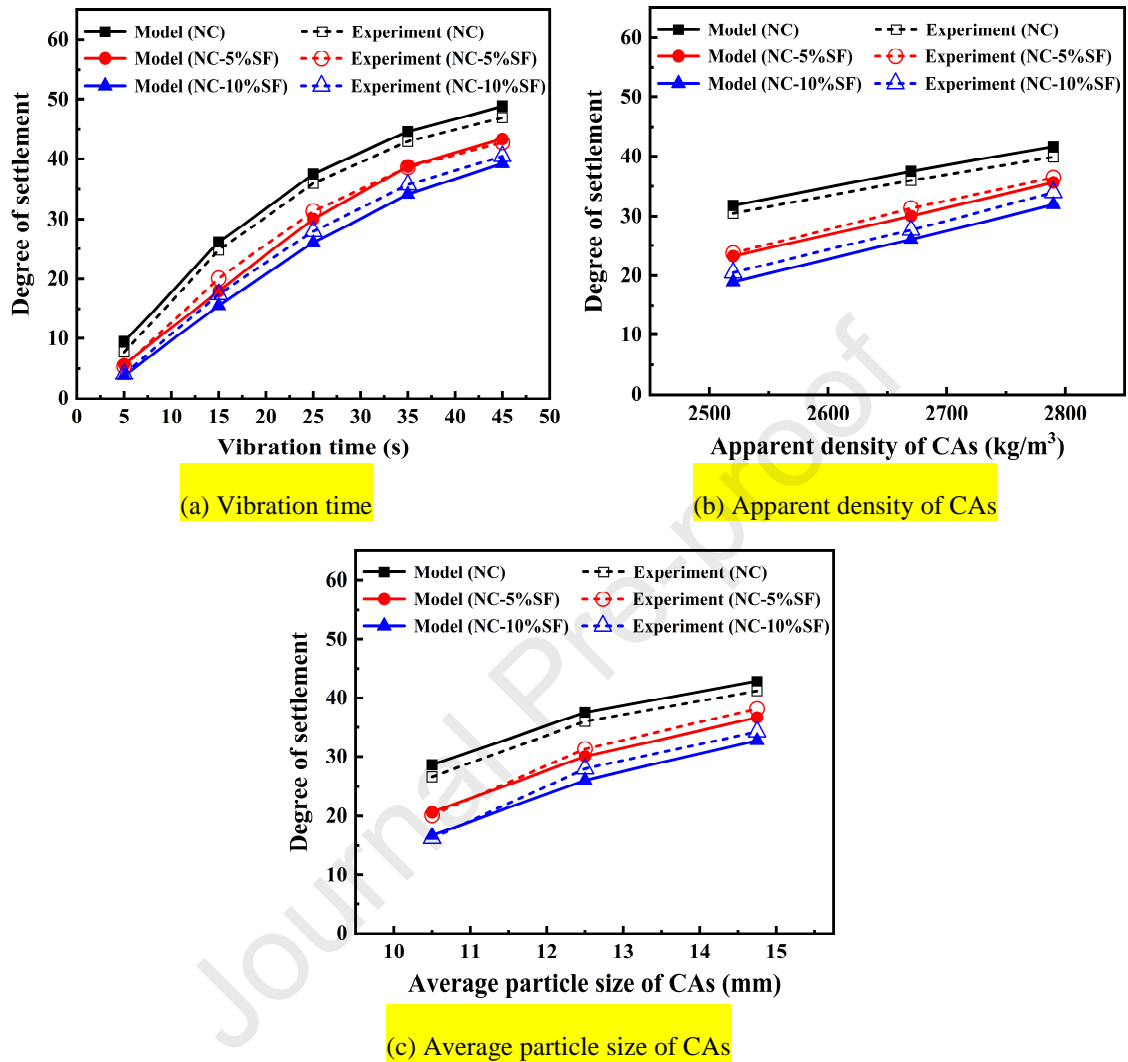
444 4.4. Verification of prediction results

445 In Sections 4.1–4.3, the numerical model was used to predict the influence of
446 vibration time, apparent density and particle size of CAs on settlement degree in the
447 three groups of concrete mixtures. Next, the validity of the proposed model based on
448 experimental results would be discussed in this section. Although the vibration time of
449 fresh concrete usually did not exceed 30 s, the tests of vibrating durations of 35 s and
450 45 s were still carried out to validate the previous prediction. In addition, the
451 limestone with apparent densities of 2520 kg/m³ and 2790 kg/m³ prepared in the
452 laboratory could be used to test the influence of the CA density on settlement. For the
453 experiment of the effect of the CA particle size, the CAs with diameters of 5–16 mm
454 and 9.5–20 mm could be obtained from original particle size (5–20 mm) through 16
455 mm and 9.5 mm size sieves, respectively.

456 The experimental results determined by the segmented sieving method were used
457 to verify the prediction results of numerical model, as presented in Fig. 14. For the
458 vibration time, the model prediction was in good agreement with the experimental
459 results as evident in Fig. 14(a). With the vibration time going on, both the settlement
460 degree and heterogeneity distribution of CAs were more pronounced. When the
461 vibration time reached a certain value, the increase of settlement degree became
462 slower due to the close packing of some CAs in the bottom layer. Similarly, when the
463 numerical method was used to predict the influence of the apparent density and
464 particle size of CAs on settlement, it also showed a good correlation with the
465 experimental results (see Fig. 14(b) and (c)), which indicated that the model was

466 applicable in this study.

467



468 Fig. 14. Experimental verification of the prediction results.

469

470 4.5. Grey relational analysis

471 The grey relational analysis table of different influencing factors is summarized
 472 in Table 6. Here, this method is used to characterize the contribution of each factor to
 473 CA settlement. The settlement degree is taken as the reference sequence. The
 474 influencing factors such as vibration time, apparent density and particle size of CAs,

475 and plastic viscosity of mixtures are taken as the comparable sequences.

476

477

Table 6 Grey relational analysis table of different influencing factors.

Group	Vibration time (s)	Apparent density of CAs (kg/m ³)	Particle size of CAs (mm)	Plastic viscosity of mixtures (Pa·s)	Degree of settlement
1	5	2670	5–20	45.0	9.4484
2	15	2670	5–20	45.0	26.1419
3	25	2670	5–20	45.0	37.5106
4	35	2670	5–20	45.0	44.6035
5	45	2670	5–20	45.0	48.8770
6	5	2670	5–20	48.4	5.6692
7	15	2670	5–20	48.4	17.9724
8	25	2670	5–20	48.4	30.0583
9	35	2670	5–20	48.4	38.7519
10	45	2670	5–20	48.4	43.3282
11	5	2670	5–20	51.3	3.7958
12	15	2670	5–20	51.3	15.5593
13	25	2670	5–20	51.3	26.0454
14	35	2670	5–20	51.3	34.1547
15	45	2670	5–20	51.3	39.2495
16	25	2520	5–20	45.0	31.8085
17	25	2790	5–20	45.0	41.6522
18	25	2520	5–20	48.4	23.2047
19	25	2790	5–20	48.4	35.6362
20	25	2520	5–20	51.3	18.9375
21	25	2790	5–20	51.3	31.9706
22	25	2670	5–16	45.0	28.0206
23	25	2670	9.5–20	45.0	42.8769
24	25	2670	5–16	48.4	20.3044
25	25	2670	9.5–20	48.4	36.6233
26	25	2670	5–16	51.3	16.4197
27	25	2670	9.5–20	51.3	32.7796
Grey relational grade	0.7392	0.6291	0.6435	0.6222	–

478

479 Assuming the reference and comparable sequences are respectively denoted as

480 $X_0(k)$ and $X_i(k)$. Before conducting a grey relational analysis, the original reference

481 and comparable sequences need to be normalized by data pre-processing, as follows:

$$482 \quad x_0(k) = \frac{X_0(k)}{\frac{1}{n} \sum_{k=1}^n X_0(k)} \quad (14)$$

$$483 \quad x_i(k) = \frac{X_i(k)}{\frac{1}{n} \sum_{k=1}^n X_i(k)} \quad (15)$$

484 where $x_0(k)$ and $x_i(k)$ are the sequences after data pre-processing, and $i=1, 2, \dots, m$ and
 485 $k=1, 2, \dots, n$.

486 When the dimensionless data are prepared, the grey relational coefficient can be
 487 derived by Eq. (16).

$$488 \quad \varepsilon_i(k) = \frac{\Delta_{\min} + \rho \Delta_{\max}}{\Delta_{0i}(k) + \rho \Delta_{\max}} \quad (16)$$

489 Here, the absolute difference between each evaluated comparable sequence and
 490 the corresponding element of reference sequence is calculated in turn, and then Δ_{\min} ,
 491 Δ_{\max} and $\Delta_{0i}(k)$ can be obtained by Eqs. (17)–(19). Moreover, ρ is called the resolution
 492 coefficient, and the smaller ρ indicates the greater resolution. In general, the value of ρ
 493 is 0.5.

$$494 \quad \Delta_{\min} = \min_i \min_k |x_0(k) - x_i(k)| \quad (17)$$

$$495 \quad \Delta_{\max} = \max_i \max_k |x_0(k) - x_i(k)| \quad (18)$$

$$496 \quad \Delta_{0i}(k) = |x_0(k) - x_i(k)| \quad (19)$$

497 As the calculated relational coefficients are not only large in quantity, but also
 498 discrete, it is impossible to directly compare them. It needs to average the relational
 499 coefficients to convert each sequence into a relational grade, as shown in Eq. (20).

$$500 \quad \gamma_i = \frac{1}{n} \sum_{k=1}^n \varepsilon_i(k) \quad (20)$$

501 where γ_i is the grey relational grade.

502 On the basis of the principle of grey relational analysis, a larger value of γ_i
503 implies that the related influencing factor has a greater impact on CA settlement. After
504 calculation, it is found that the grey relational grades of the influencing factors are γ
505 (vibration time) = 0.7392, γ (apparent density of CAs) = 0.6291, γ (particle size of
506 CAs) = 0.6435, and γ (plastic viscosity of mixtures) = 0.6222, respectively. It means
507 that the order of these four influencing factors for the contribution of CA settlement in
508 this study is vibration time > particle size of CAs > apparent density of CAs > plastic
509 viscosity of mixtures. This supports the general observation that vibration time should
510 be limited in practical applications.

511

512 **5. Conclusions**

513 In this study, an experimental and numerical work of CA settlement in vibrated
514 fresh concrete was investigated. Based on the previous results and discussion, the
515 following conclusions could be drawn:

- 516 1) The distribution profiles of CAs in vibrated concrete presented a growing
517 tendency towards the bottom layer with vibration time. After a certain period of
518 vibrating, some CAs in the bottom part formed the close packing, and the growth
519 of the non-uniform distribution gradually began to weaken.
- 520 2) Due to the opacity of concrete, the proposed 3-D model for fresh concrete could
521 be used as a potential approach to visualize the CA movement. For the top part of
522 specimen, the visual analysis showed that a surface layer enriched in cement
523 mortars formed in this area, where only contained few of small-sized CAs.

- 524 3) The heterogeneity of concrete had a positive correlation with the density
525 difference between CAs and mortars and the particle size of CAs. SF, as a mineral
526 admixture to improve the plastic viscosity of mixtures, could effectively reduce
527 the settlement and segregation of fresh cement-based materials.
- 528 4) The segmented sieving method was performed to assess the validity of numerical
529 model. The results indicated that the model prediction was well verified by the
530 experimental results. The methodology proposed in this study provided an
531 effective tool to further understand the settlement behaviour of CAs.
- 532 5) Grey relational analysis demonstrated that the vibration time had the greatest
533 influence on CA settlement, followed by the particle size of CAs. Compared with
534 the former two influencing factors, the apparent density of CAs and the plastic
535 viscosity of mixtures contributed a little to the settlement.

536

537 **Acknowledgments**

538 This work was funded by the National Natural Science Foundation of China
539 [51978396] and the Shanghai Rising-Star Program, China [19QA1404700].

540

541 **References**

- 542 [1] K. Kovler, N. Roussel, Properties of fresh and hardened concrete, *Cem. Concr. Res.* 41 (7)
543 (2011) 775–792.
- 544 [2] N. Roussel, A theoretical frame to study stability of fresh concrete, *Mater. Struct.* 39 (1) (2006)
545 81–91.

- 546 [3] D. Jiao, C. Shi, Q. Yuan, X. An, Y. Liu, H. Li, Effect of constituents on rheological properties
547 of fresh concrete-A review, *Cem. Concr. Compos.* 83 (2017) 146–159.
- 548 [4] G. Torelli, J.M. Lees, Fresh state stability of vertical layers of concrete, *Cem. Concr. Res.* 120
549 (2019) 227–243.
- 550 [5] W.S. Alyhya, S. Kulasegaram, B.L. Karihaloo, Simulation of the flow of self-compacting
551 concrete in the V-funnel by SPH, *Cem. Concr. Res.* 100 (2017) 47–59.
- 552 [6] J. Zhang, X. Gao, Y. Su, Influence of poker vibration on aggregate settlement in fresh concrete
553 with variable rheological properties, *J. Mater. Civ. Eng.* 31 (7) (2019) 04019128.
- 554 [7] W. Yan, W. Cui, L. Qi, Effect of aggregate gradation and mortar rheology on static
555 segregation of self-compacting concrete, *Constr. Build. Mater.* 259 (2020) 119816.
- 556 [8] M.I. Safawi, I. Iwaki, T. Miura, A study on the applicability of vibration in fresh high fluidity
557 concrete, *Cem. Concr. Res.* 35 (9) (2005) 1834–1845.
- 558 [9] G.H. Tattersall, P.H. Baker, The effect of vibration on the rheological properties of fresh
559 concrete, *Mag. Concr. Res.* 40 (143) (1988) 79–89.
- 560 [10] G.H. Tattersall, P.H. Baker, An investigation into the effect of vibration on the workability of
561 fresh concrete using a vertical pipe apparatus, *Mag. Concr. Res.* 41 (146) (1989) 3–9.
- 562 [11] C. Hu, F. de Larrard, The rheology of fresh high-performance concrete, *Cem. Concr. Res.* 26
563 (2) (1996) 283–294.
- 564 [12] B. Esmailkhanian, K.H. Khayat, A. Yahia, D. Feys, Effects of mix design parameters and
565 rheological properties on dynamic stability of self-consolidating concrete, *Cem. Concr. Compos.*
566 54 (2014) 21–28.

- 567 [13] C. Pichler, R. Rock, R. Lackner, Apparent power-law fluid behavior of vibrated fresh
568 concrete: Engineering arguments based on Stokes-type sphere viscometer measurements, *J.*
569 *Non-Newtonian Fluid Mech.* 240 (2017) 44–55.
- 570 [14] W. Zhu, J.C. Gibbs, P.J.M. Bartos, Uniformity of in situ properties of self-compacting
571 concrete in full-scale structural elements, *Cem. Concr. Compos.* 23 (1) (2001) 57–64.
- 572 [15] A. Leemann, B. Munch, P. Gasser, L. Holzer, Influence of compaction on the interfacial
573 transition zone and the permeability of concrete, *Cem. Concr. Res.* 36 (8) (2006) 1425–1433.
- 574 [16] D.K. Panesar, B. Shindman, The effect of segregation on transport and durability properties
575 of self consolidating concrete, *Cem. Concr. Res.* 42 (2) (2012) 252–264.
- 576 [17] X. Gao, J. Zhang, Y. Su, Influence of vibration-induced segregation on mechanical property
577 and chloride ion permeability of concrete with variable rheological performance, *Constr. Build.*
578 *Mater.* 194 (2019) 32–41.
- 579 [18] Y. Cai, W. Zhang, L. Yu, M. Chen, C. Yang, R. François, K. Yang, Characteristics of the
580 steel-concrete interface and their effect on the corrosion of steel bars in concrete, *Constr. Build.*
581 *Mater.* 253 (2020) 119162.
- 582 [19] W. Zhang, R. François, Y. Cai, J.-P. Charron, L. Yu, Influence of artificial cracks and
583 interfacial defects on the corrosion behavior of steel in concrete during corrosion initiation under a
584 chloride environment, *Constr. Build. Mater.* 253 (2020) 119165.
- 585 [20] Y. Cai, W. Zhang, C. Yang, R. François, L. Yu, M. Chen, H. Chen, H. Yang, Evaluating the
586 chloride permeability of steel–concrete interface based on concretes of different stability, *Struct.*
587 *Concr.* (2020) 1–14.

- 588 [21] C. Wu, C. Chen, C. Cheeseman, Size effects on the mechanical properties of 3D printed
589 plaster and PLA parts, *J. Mater. Civ. Eng.* 33 (7) (2021) 04021152.
- 590 [22] M.F. Petrou, K.A. Harries, F. Gadala-Maria, V.G. Kolli, A unique experimental method for
591 monitoring aggregate settlement in concrete, *Cem. Concr. Res.* 30 (5) (2000) 809–816.
- 592 [23] J.A. Koch, D.I. Castaneda, R.H. Ewoldt, D.A. Lange, Vibration of fresh concrete understood
593 through the paradigm of granular physics, *Cem. Concr. Res.* 115 (2019) 31–42.
- 594 [24] Z. Tian, X. Li, F. Zhu, Z. Peng, Experimental simulation study on aggregate motion of
595 rheological concrete, *J. Build. Mater.* 19 (1) (2016) 22–28.
- 596 [25] F.S. Barbosa, A.L. Beaucour, M.C.R. Farage, S. Ortola, Image processing applied to the
597 analysis of segregation in lightweight aggregate concretes, *Constr. Build. Mater.* 25 (8) (2011)
598 3375–3381.
- 599 [26] I. Navarrete, M. Lopez, Understanding the relationship between the segregation of concrete
600 and coarse aggregate density and size, *Constr. Build. Mater.* 149 (2017) 741–748.
- 601 [27] M. Nili, M. Razmara, M. Sadeghi, M. Razmara, Automatic image analysis process to
602 appraise segregation resistance of self-consolidating concrete, *Mag. Concr. Res.* 70 (8) (2018)
603 390–399.
- 604 [28] M. Benaicha, O. Jalbaud, X. Roguiez, A.H. Alaoui, Y. Burtshell, Prediction of
605 Self-Compacting Concrete homogeneity by ultrasonic velocity, *Alex. Eng. J.* 54 (4) (2015) 1181–
606 1191.
- 607 [29] K.H. Khayat, T.V. Pavate, J. Assaad, C. Jolicoeur, Analysis of variations in electrical
608 conductivity to assess stability of cement-based materials, *ACI Mater. J.* 100 (4) (2003) 302–310.

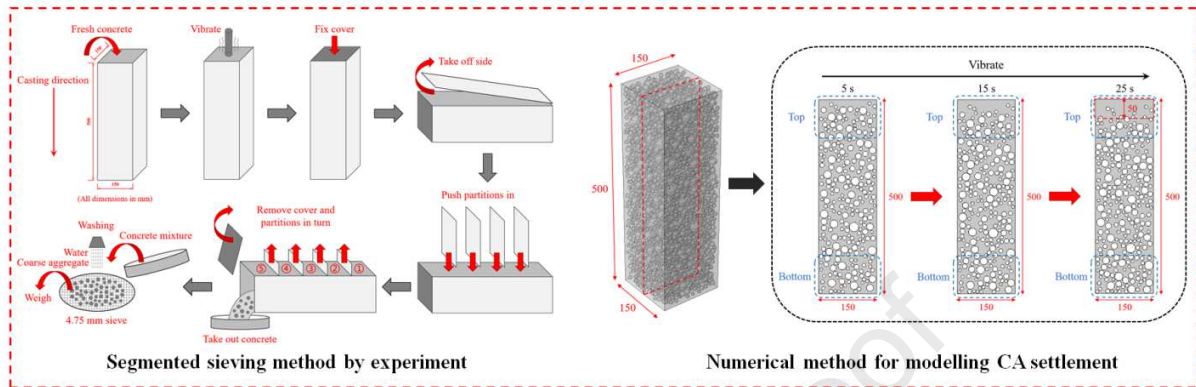
- 609 [30] Y. Vanhove, C. Djelal, G. Schwendenmann, P. Brisset, Study of self consolidating concretes
610 stability during their placement, *Constr. Build. Mater.* 35 (2012) 101–108.
- 611 [31] H.S. Gokce, B.C. Ozturk, N.F. Çam, O. Andiç-Çakir, Gamma-ray attenuation coefficients
612 and transmission thickness of high consistency heavyweight concrete containing mineral
613 admixture, *Cem. Concr. Compos.* 92 (2018) 56–69.
- 614 [32] F. Mahmoodzadeh, S.E. Chidiac, Rheological models for predicting plastic viscosity and
615 yield stress of fresh concrete, *Cem. Concr. Res.* 49 (2013) 1–9.
- 616 [33] J. Peng, D. Deng, Z. Liu, Q. Yuan, T. Ye, Rheological models for fresh cement asphalt paste,
617 *Constr. Build. Mater.* 71 (2014) 254–262.
- 618 [34] V. Mechtcherine, S. Shyshko, Simulating the behaviour of fresh concrete with the Distinct
619 Element Method – Deriving model parameters related to the yield stress, *Cem. Concr. Compos.* 55
620 (2015) 81–90.
- 621 [35] K. Vance, G. Sant, N. Neithalath, The rheology of cementitious suspensions: A closer look at
622 experimental parameters and property determination using common rheological models, *Cem.*
623 *Concr. Compos.* 59 (2015) 38–48.
- 624 [36] B. Il Choi, J.H. Kim, T.Y. Shin, Rheological model selection and a general model for
625 evaluating the viscosity and microstructure of a highly-concentrated cement suspension, *Cem.*
626 *Concr. Res.* 123 (2019) 105775.
- 627 [37] Y. Liu, C. Shi, Q. Yuan, X. An, L. Zhu, B. Wu, The rotation speed-torque transformation
628 equation of the Robertson-Stiff model in wide gap coaxial cylinders rheometer and its applications
629 for fresh concrete, *Cem. Concr. Compos.* 107 (2020) 103511.

- 630 [38] M.I. Safawi, I. Iwaki, T. Miura, The segregation tendency in the vibration of high fluidity
631 concrete, *Cem. Concr. Res.* 34 (2) (2004) 219–226.
- 632 [39] M.F. Petrou, B.L. Wan, F. Gadala-Maria, V.G. Kolli, K.A. Harries, Influence of mortar
633 rheology on aggregate settlement, *ACI Mater. J.* 97 (4) (2000) 479–485.
- 634 [40] Y.A. Abebe, L. Lohaus, Rheological characterization of the structural breakdown process to
635 analyze the stability of flowable mortars under vibration, *Constr. Build. Mater.* 131 (2017) 517–
636 525.
- 637 [41] T.R. Muzenda, P. Hou, S. Kawashima, T. Sui, X. Cheng, The role of limestone and calcined
638 clay on the rheological properties of LC3, *Cem. Concr. Compos.* 107 (2020) 103516.
- 639 [42] D. Kong, D.J. Corr, P. Hou, Y. Yang, S.P. Shah, Influence of colloidal silica sol on fresh
640 properties of cement paste as compared to nano-silica powder with agglomerates in micron-scale,
641 *Cem. Concr. Compos.* 63 (2015) 30–41.
- 642 [43] J.J. Assaad, Correlating thixotropy of self-consolidating concrete to stability, formwork
643 pressure, and multilayer casting, *J. Mater. Civ. Eng.* 28 (10) (2016) 04016107.
- 644 [44] S. Zhuang, Q. Wang, Inhibition mechanisms of steel slag on the early-age hydration of
645 cement, *Cem. Concr. Res.* 140 (2021) 106283.
- 646 [45] L.-X. Mao, Z. Hu, J. Xia, G.-L. Feng, I. Azim, J. Yang, Q.-F. Liu, Multi-phase modelling of
647 electrochemical rehabilitation for ASR and chloride affected concrete composites, *Compos. Struct.*
648 207 (2019) 176–189.
- 649 [46] Q.-F. Liu, M.F. Iqbal, J. Yang, X.-Y. Lu, P. Zhang, M. Rauf, Prediction of chloride
650 diffusivity in concrete using artificial neural network: Modelling and performance evaluation,
651 *Constr. Build. Mater.* 268 (2021) 121082.

- 652 [47] C.-L. Zhang, W.-K. Chen, S. Mu, B. Šavija, Q.-F. Liu, Numerical investigation of external
653 sulfate attack and its effect on chloride binding and diffusion in concrete, *Constr. Build. Mater.*
654 285 (2021) 122806.
- 655 [48] F. de Larrard, C. Hu, T. Sedran, J.C. Sztikar, M. Joly, F. Claux, F. Derkx, A new rheometer
656 for soft-to-fluid fresh concrete, *ACI Mater. J.* 94 (3) (1997) 234–243.
- 657 [49] P.F.G. Banfill, Y. Xu, P.L.J. Domone, Relationship between the rheology of unvibrated fresh
658 concrete and its flow under vibration in a vertical pipe apparatus, *Mag. Concr. Res.* 51 (3) (1999)
659 181–190.
- 660 [50] Z. Li, G. Cao, Rheological behaviors and model of fresh concrete in vibrated state, *Cem.*
661 *Concr. Res.* 120 (2019) 217–226.
- 662 [51] J.-Y. Petit, E. Wirquin, Y. Vanhove, K.H. Khayat, Yield stress and viscosity equations for
663 mortars and self-consolidating concrete, *Cem. Concr. Res.* 37 (5) (2007) 655–670.
- 664 [52] A. Leemann, F. Winnefeld, The effect of viscosity modifying agents on mortar and concrete,
665 *Cem. Concr. Compos.* 29 (5) (2007) 341–349.
- 666 [53] S. Diamond, J.D. Huang, The ITZ in concrete – a different view based on image analysis and
667 SEM observations, *Cem. Concr. Compos.* 23 (2–3) (2001) 179–188.
- 668 [54] Q.-F. Liu, D. Easterbrook, J. Yang, L.-Y. Li, A three-phase, multi-component ionic transport
669 model for simulation of chloride penetration in concrete, *Eng. Struct.* 86 (2015) 122–133.
- 670 [55] Q.-F. Liu, G.-L. Feng, J. Xia, J. Yang, L.-Y. Li, Ionic transport features in concrete
671 composites containing various shaped aggregates: a numerical study, *Compos. Struct.* 183 (2018)
672 371–380.

- 673 [56] W.A. Megid, K.H. Khayat, Effect of concrete rheological properties on quality of formed
674 surfaces cast with self-consolidating concrete and superworkable concrete, *Cem. Concr. Compos.*
675 93 (2018) 75–84.
- 676 [57] J.J. Assaad, J. Harb, Surface settlement of cementitious-based materials determined by
677 oedometer testing, *Mater. Struct.* 44 (2011) 845–856.
- 678 [58] B.M. Aissoun, J.-L. Gallias, K.H. Khayat, Influence of formwork material on transport
679 properties of self-consolidating concrete near formed surfaces, *Constr. Build. Mater.* 146 (2017)
680 329–337.
- 681 [59] I. Navarrete, M. Lopez, Estimating the segregation of concrete based on mixture design and
682 vibratory energy, *Constr. Build. Mater.* 122 (2016) 384–390.
- 683 [60] K.S. Chia, C.C. Kho, M.H. Zhang, Stability of fresh lightweight aggregate concrete under
684 vibration, *ACI Mater. J.* 102 (5) (2005) 347–354.
- 685 [61] Y. Ke, A.L. Beaucour, S. Ortola, H. Dumontet, R. Cabrillac, Influence of volume fraction and
686 characteristics of lightweight aggregates on the mechanical properties of concrete, *Constr. Build.*
687 *Mater.* 23 (2009) 2821–2828.
- 688 [62] L. Shen, H.B. Jovein, Q. Wang, Correlating aggregate properties and concrete rheology to
689 dynamic segregation of self-consolidating concrete, *J. Mater. Civ. Eng.* 28 (1) (2016) 04015067.
- 690 [63] M.F. Iqbal, Q.-F. Liu, I. Azim, X. Zhu, J. Yang, M.F. Javed, M. Rauf, Prediction of
691 mechanical properties of green concrete incorporating waste foundry sand based on gene
692 expression programming, *J. Hazard. Mater.* 384 (2020) 121322.
- 693 [64] J.J. Assaad, Influence of recycled aggregates on dynamic/static stability of self-consolidating
694 concrete, *J. Sustainable Cem.-Based Mater.* 6 (6) (2017) 345–365.

- 695 [65] W. Cui, W.-S. Yan, H.-F. Song, X.-L. Wu, DEM simulation of SCC flow in L-Box set-up:
696 Influence of coarse aggregate shape on SCC flowability, *Cem. Concr. Compos.* 109 (2020)
697 103558.
- 698 [66] M.F. Iqbal, M.F. Javed, M. Rauf, I. Azim, M. Ashraf, J. Yang, Q.-F. Liu, Sustainable
699 utilization of foundry waste: Forecasting mechanical properties of foundry sand based concrete
700 using multi-expression programming, *Sci. Total Environ.* 780 (2021) 146524.

HIGHLIGHTS**Coarse aggregate settlement in fresh concrete under vibration**

- A rheological problem of cement-based materials has been studied both experimentally and numerically.
- The numerical method is developed for the first time to investigate the settlement behaviour of CAs in vibrated concrete.
- The validity of the model prediction is verified by the experimental results, based on the segmented sieving method.
- Grey relational analysis is performed to study the influence of related factors on the settlement of CAs.

Declaration of interests

The authors declare that they have no known competing financial interests or personal relationships that could have appeared to influence the work reported in this paper.

The authors declare the following financial interests/personal relationships which may be considered as potential competing interests:



Qing-feng LIU